Microporous Membranes of Isotactic Poly(4-methyl-1-pentene) from a Melt-Extrusion Process. II. Effects of Thermal Annealing and Stretching on Porosity

MATTHEW B. JOHNSON, GARTH L. WILKES

Virginia Tech, Polymer Materials and Interfaces Laboratory and Department of Chemical Engineering, Blacksburg, Virginia 24061

Received 19 May 2001; accepted 4 June 2001

ABSTRACT: A two-part study utilizing isotactic poly(4-methyl-1-pentene) (PMP) was undertaken to investigate a three-stage process (melt-extrusion/annealing/uniaxial stretching) (MEAUS) utilized to produce microporous films. In this report, the thermal-annealing (second stage) and subsequent uniaxial-stretching (third stage) results of selected PMP films from three resins, labeled A, B, and C, are discussed. From sequential analysis of the effect each stage had on the resulting microporosity, it was discovered that the melt-extruded precursor morphology and orientation, as a consequence of the first-stage extrusion parameters and resin characteristics, were crucial to controlling the membrane permeability. The annealing parameters were also critical, where a temperature of 205°C applied for 20 min under no tension was the optimum annealing condition for producing highly microporous PMP films upon stretching. For the conditions studied, the stretching parameters that were found to be the optimum for producing the desired characteristics in the final film were cold- and hot-stretch temperatures of 70 and 180°C, respectively. The cold- and hot-stretch extension levels concluded to be the best were a cold-stretch extension of 80%, followed by hot stretching to 90%, and, thus, a total overall extension level of 170% for the processing window studied. However, these results were only with respect to resin A films, while resin B and C samples could not be produced into microporous films via the MEAUS process. © 2002 Wiley Periodicals, Inc. J Appl Polym Sci 84: 1076–1100, 2002; DOI 10.1002/app.10395

INTRODUCTION

Polymeric microporous membranes are produced by a variety of methods with one of these composed of three stages: melt-extrusion, thermal annealing, and uniaxial stretching, which will be designated in this article as the MEAUS method. Although there has been some published literature[1–3] and several patents,[4–7] describing the MEAUS procedures for producing microporous membranes, a sequential study covering this method for PMP has never appeared in the published literature. This is true even though the underlying mechanisms and the means to attain the desired outcomes at each stage are generally known. For example, many of the references listed above describe the MEAUS process as being the deformation of a "hard-elastic" semicrystalline polymeric material. It is recognized in the literature that these materials emanate from semicrystalline materials possessing a parallel or planar stacked lamellar morphology. Additionally, this type of lamellar arrangement is a con-

Correspondence to: G. L. Wilkes.
Contract grant sponsor: Celgard Corp. LLC.

Journal of Applied Polymer Science, Vol. 84, 1076–1100 (2002)

sequence of a row-nucleated morphology created by the appropriate melt-flow stress conditions in the course of extrusion.

In the first article[8] of this two-part investigation, the melt-extrusion results of three poly(4-methyl-1-pentene) (PMP) resins (A, B, and C) were discussed. The resins differed mainly in the weight-average molecular weight (M_w), although resin B had approximately double (6.5 wt %) the level of a 1-olefin comonomer (believed to be 1-decene) possessed by resins A or C. Upon melt-extrusion, precursor films possessing stacked lamellar morphologies were obtained from each resin. In the case of resin A, the films all possessed parallel planar lamellae textures for the process window studied. However, only select films from the other two resins (B and C) were characterized by planar lamellar structures. The chain-axis crystal orientation with respect to the machine direction (MD) was also determined for these precursors utilizing wide-angle X-ray scattering (WAXS). When the precursors were melt-extruded under similar conditions, it was found that resin A films possessed the highest chain-axis orientation followed by the resin B films and, lastly, the resin C films. These morphological and orientation results were concluded to be a consequence of the process conditions and melt-relaxation times, where the highest M_w resin (A) possessed the longest melt-relaxation time, followed by the intermediate M_w resin (B) and the lowest M_w resin (C).

To generate microporosity in these melt-extruded precursor films, an annealing stage is also required.[9] Its utility is believed to be in the promotion of small-scale structural modifications in both the crystalline and amorphous phases, accomplished in the MEAUS process through control of the annealing temperature (T_a), time (t_a), and tension level (percent extension) applied to the film during this stage. The desired modifications in the crystalline regions are thickening and perfection of the lamellae promoted at annealing temperatures below the melting point (T_m) but above the glass transition temperature (T_g). In the amorphous regions, the interlamellar linkages (tie chains) are also thought to become less taut and in some cases are believed to be "reeled-in," thus potentially leading to fewer tie chains.[10] The effects just described are possible for a semicrystalline polymer, *only if it possesses an* α_c *relaxation*,[10–12] and, in addition, according to Rault,[10] only if it is annealed at a temperature above the maximum value of the relaxation ($T_{\alpha c}$),

The α_c relaxation is associated with chain-axis translational mobility of the nonchemical defects in the crystal lattice. Since polymeric relaxations are not only temperature-dependent but also frequency-dependent, this particular value ($T_{\alpha c}$) is somewhat arbitrary but can be determined via dynamic mechanical spectroscopy (DMS) for a given frequency. The existence of such a relaxation is "necessary, but not sufficient"[13] for lamellae to thicken because the presence of noncrystallizable units along the polymer backbone (comonomer, branches, etc.) and highly entangled interlamellar regions and the nature of the morphology may affect the crystalline thickening process.[13] Boyd suggested that the α_c relaxation is only a characteristic of polymers that cannot be rapidly cooled into a completely amorphous material. He categorized such polymers as "high" crystalline materials.[12,14] Linear high-density polyethylene (HDPE) fits this classification based upon its relatively fast crystallization rate and reported α_c relaxation(s).[11,12,15–17] Both isotactic polypropylene (iPP)[10,16] and isotactic PMP[10] are also known to each possess an α_c relaxation. In fact, microporous membranes are commercially available from HDPE and iPP produced via the MEAUS process that is under discussion.[18]

The ability of the chains to translate through the crystalline lamellae also enables polymers possessing the α_c relaxation to be drawn or deformed to higher levels than those that do not possess this relaxation. In fact, it has been recognized that ultradrawing and solid-state processing of semicrystalline polymers possessing an α_c relaxation are possible, and the polymers that do not have this crystalline mobility are unable to undergo either ultradrawing or solid-state processing.[19–21] Ultradrawing is defined as achieving draw ratios (L/L_0) greater than 20, where L is the final sample length and L_0 is the initial sample length. Higher extensibility also permits greater levels of lamellar separation (splaying) and subsequent local drawing in some cases upon stretching, the third stage of the MEAUS process. This third stage is composed of two stretching steps followed by a thermal-relaxation/heat-setting step. The first step is designated the "cold" stretch, while the second is the "hot" stretch. The cold-stretch temperature (T_{cs}) generally occurs above the polymer T_g but below the hot-stretch temperature (T_{hs}), which itself is below the annealing temperature of the prior stage but still in the upper temperature range of the α_c relaxation for a given polymer. The extension levels utilized

during the cold-stretch (% CS) and hot-stretch (% HS) steps also need to be considered. The stretching directions in both steps are along the MD of the annealed film, that is, perpendicular to the stacked lamellae. Cold stretching is utilized to "nucleate" the micropores via a ductile drawing of the amorphous and crystalline phases. The hot-stretch step further splays the lamellae (i.e., increases the pore size) via a partial ductile drawing of the crystal phase. Following the stretching steps, the thermal-relaxation/heat-setting step is employed to allow partial recovery of the film in the first case, while the latter is to impart dimensional stability after removal from the stretching oven and stretching apparatus. As was observed in a previous dissertation study[3] using melt-extruded HDPE films,[2] the uniformity and number of these microvoids can be influenced through the processing conditions at each stage (melt-extrusion, annealing, and stretching). Since control of the micropore structure and the film permeability is highly desirable, it is essential to understand the variables that can alter the quality of the microporosity produced upon annealing and subsequently stretching the melt-extruded films.

As stated above, this report is the second in the series that presents findings from the sequential study of the MEAUS process utilizing PMP. It is the main goal of the overall study was that the information obtained will lead to a better understanding of how to control the microporous behavior of the final stretched PMP membranes. This will be accomplished by the sequential analysis of the results from each of the three process stages. The results of the first stage (melt-extrusion) have already been presented and discussed[8] with a limited reiteration above. In this second article, the annealing (second stage) and stretching (third stage) results are presented for selected melt-extruded PMP films from that earlier work. Furthermore, the same sample designation will be utilized for continuity. Specifically, in this report, we will address samples, A1, A2, B1, and C1, that were extruded under the conditions stated in Tables 2–4 from ref. 8. These melt-extruded precursor films were chosen based upon their morphological features and orientation state in order to investigate the effects of specific annealing (T_a, t_a, and tension) and stretching process variables (T_{cs}, % CS, T_{hs} % HS). In our first report,[8]the authors suggested some prerequisites for the production of a membrane with a high concentration of micropores uniformly distributed throughout the film. Two of the prerequisites were that the precursor should possess a parallel planar stacked lamellar morphology and a relatively high crystalline orientation. In fact, films A1, A2, and B1 each possessed these precursor characteristics, while sample C1 had a lower crystalline orientation, as reviewed shortly. Thus, the precursor films based on resin A (A1 and A2) will be the particular focus of this report, and samples B1 and C1 will be analyzed to a lesser extent.

Table I Molecular Weight Characteristics for the Three PMP Resins Studied

Sample	M_n (kg/mol)	M_w (kg/mol)	M_w/M_n
Resin A	44.5	460	10.3
Resin B	58.0	360	6.2
Resin C	36.9	290	7.8

EXPERIMENTAL

Materials

Melt-extruded precursor films made previously via a tubular blown-film process were selected from each of the three PMP resins A, B, and C. Besides obvious molecular weight differences, listed in Table I, resins A and C are believed to possess approximately the same amount of 1-decene, about 3.2 wt %. Additionally, resin B was determined to have nearly double this amount, as measured via solution NMR.[22] The additional comonomer content of resin B will be shown later to influence the α_c relaxation of resin B precursors.

Structural and Optical Techniques Utilized

WAXS

WAXS studies were performed on a Philips tabletop X-ray generator Model PW1720 equipped with a standard vacuum-sealed Warhus photographic pinhole camera. The X-ray beam was of CuKα radiation, λ = 1.544 Å, and was collimated to a beam diameter of 0.020 in. (0.508 mm).

Since the extrusion led to planar extensional flow along the MD, this promoted uniaxial orientation behavior with respect to the MD axis.[2] As a result, the nature of the crystalline orientation distribution (orientation function) need only be obtained by examination of the azimuthal angle dependence of different reflections arising from

standard flat-plate WAXS patterns. The orientation function utilized was the Hermans' orientation function (f_H)[23]:

$$f_H = \frac{(3\langle\cos^2\theta\rangle - 1)}{2} \quad (1)$$

where θ is the angle between the chain or specific unit cell axis and a chosen reference axis, which is the MD in our case. The procedural details for determining the crystalline orientation (f_c) in the PMP films discussed in this article was given in our first report.[8]

Infrared Linear Dichroism

A Nicolet 510 FTIR spectrometer equipped with a wire grid polarizer was used for determining FTIR dichroism, D, which is defined as

$$\mathrm{D} = \frac{A_\parallel}{A_\perp} \quad (2)$$

where $A_\parallel$ is the absorption parallel and $A_\perp$ is the absorption perpendicular to a specific reference axis. For uniaxial orientation, the dichroic ratio is related to the Hermans' orientation function by the following relationship:

$$f_H = \left[\frac{(D_0 + 2)}{(D_0 - 1)}\right]\left[\frac{(D - 1)}{(D + 2)}\right] \quad (3)$$

where $D_0 = 2\cot^2\alpha$, and the value for α is the angle between the chromophore transition moment and the chain axis. For PMP, a vibration specific to a single phase is not known. He and Porter,[24] however, used the dichroism of the 918-cm^{-1} band, a rocking mode vibration from two methyl groups,[25] to follow the sample orientation as a function of extension.

Atomic Force Microscopy (AFM)

AFM micrographs were obtained with the use of a Digital Instruments Nanoscope III scanning probe microscope operated in a TappingMode™. Nanosensor TESP single-beam cantilever tips possessing force constants of 35 ± 7 N/m and oscillating at frequencies of about 290 kHz were used. The films were placed upon glass slides using double-stick tape with raster scanning of the sample done parallel to the MD of the film.

Transmission Electron Microscopy (TEM) and Scanning Electron Microscopy (SEM)

TEM micrographs were taken with a Philips EM-420 scanning transmission electron microscope (STEM) utilizing the procedures presented in the initial report for this study.[8]

Differential Scanning Calorimetry (DSC)

DSC measurement was performed with a Perkin–Elmer DSC-7. Heating scans were conducted utilizing the procedures presented in our initial report.[8]

Dynamic Mechanical Spectroscopy (DMS)

Dynamic mechanical testing was carried out on a Seiko Instruments DMS 210. The samples were tested in the tensile mode using samples approximately 0.0254 mm thick, 10 mm long, and 6 mm wide. The DMS experiments were performed at a frequency of 1 Hz using a heating rate of 2°C/min under a N_2 atmosphere.

Gurley Instrument and Film Thickness

Film porosity was determined by measuring the stretched film permeability given in terms of a parameter called the Gurley number. The Gurley number is defined as the time required for 10 cc of air to pass through a 1-in. square section of film at a constant pressure of 12.2 in. of H_2O, where the Gurley number is given in units of seconds. It is thus an inverse index of permeability where a greater Gurley number implies a lower permeability.[3] The Gurley number measurements were performed using a Gurley densometer Model 4150. In this report, a "quality" microporous film is defined as a film possessing a Gurley number less than 100 s. A *minimum* of six Gurley measurements were made for each stretched film. Film-thickness measurements were carried out on a Series 400 precision micrometer.

RESULTS

As previously stated, four extruded precursor films, A1, A2, B1, and C1, previously made using a tubular blown film process (blowup ratio of unity) were utilized for this study, and all four films possessed stacked lamellar morphologies that were in some cases planar. Table II provides this information along with other pertinent film

Table II Pertinent Characteristics of the Precursor Films Utilized in This Study

Sample	Lamellar Morphology	f_c	X_c (%)	T_m (°C)
A1	Planar	0.89	63	229
A2	Partially twisted	0.83	62	231
B1	Planar	0.84	42	221
C1	Partially twisted	0.67	63	231

characteristics. Because of the large number of annealing and stretching variable combinations utilized, only selected annealing and stretching results will be presented that are, in general, representative of most of the PMP films studied.

Annealing (Stage Two)

The annealing temperatures studied were selected based upon the range of temperatures encompassing the PMP mechanical α_c relaxation, as expressed by tan δ, for the resin A or C precursors, as shown in Figure 1. It is observed that the range of temperatures encompassing the α_c relaxation for either the resin A or C film is approximately 60–235°C, with the maximum (T_{α_c})) occurring at about 140°C. In fact, the α_c relaxations of these two films are similar in shape (not magnitude). In contrast, film B1 possesses an α_c relaxation that is partially convoluted with the T_g and is likely a consequence of the crystalline imperfection due to the additional comonomer present in resin B. From this analysis of the PMP films, annealing temperatures equal to 145, 160, 180, and 205°C were selected. The upper annealing temperatures were also slightly below and above the approximate onset of the PMP melting endotherm—see Figure 2.

The annealing times employed were 5, 10, and 20 min. These were chosen in light of feasible industrial processing times. The tension level was divided into two main categories: annealing without tension (free-anneal or 0% tension) and annealing under a specified level of tension, where in the case of the latter, the levels of tension (extension) were 3, 9, and 15%. These levels were applied during the annealing stage with a small mechanical stretching device. This device was the same one employed in the stretching stage. The effect of tension during annealing is important to the industrial-scale process, where a certain amount of film extension (tension) is applied to keep the film taut while it proceeds through the annealing oven in a continuous process. The level of tension may alter the film morphology and crystalline orientation prior to stretching, which, in turn, can affect the microporosity and the morphology of the microporous film. The specific levels of tension utilized for the present study are, in

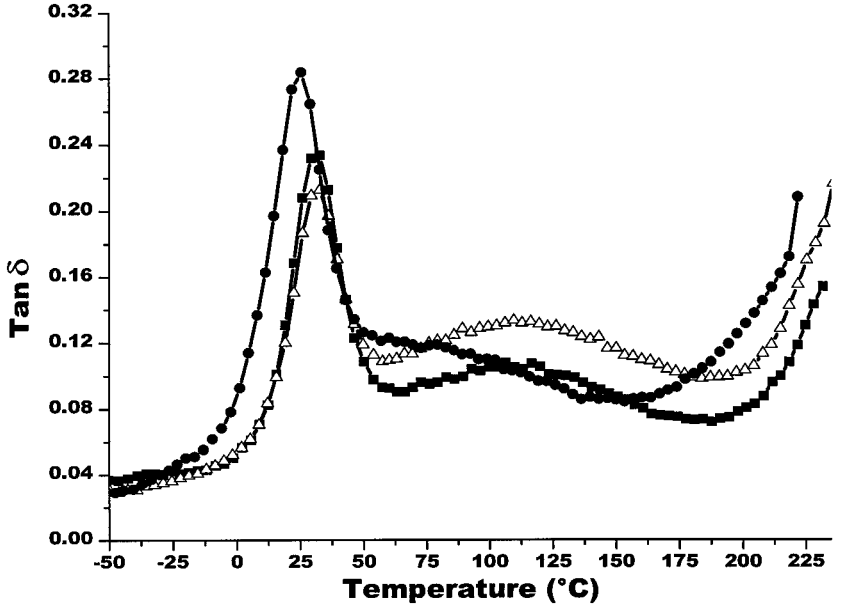

Figure 1 Tan δ as a function of temperature for PMP resins: (-■-) A; (-●-) B; (-△-) C. These data were obtained utilizing a heating rate of 2°C/min and a frequency of 1.0 Hz.

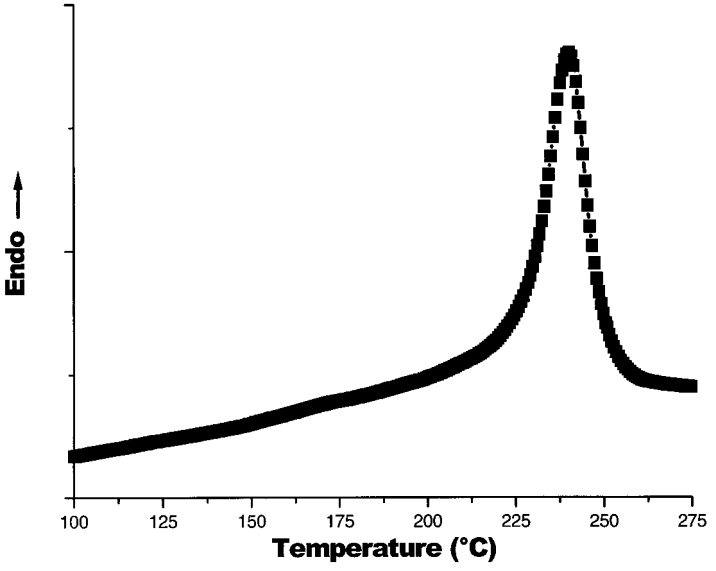

Figure 2 DSC heating scan of PMP resin A where a heating rate of 30°C/min was employed.

part, based upon the previous work of Yu on HDPE films,[3] where tension was observed to affect the annealed film morphology and crystal orientation (f_c), as discussed later.

In Figure 3(a–d), the WAXS diffraction patterns are displayed for four A1 films: the precursor (i.e., nonannealed), a free-annealed film, a film annealed under 3% tension, and a film annealed under 15% extension, respectively. The annealed films presented in this figure utilized an annealing temperature equal to 205°C for a time of 20 min. It is observed that the azimuthal dependence of the (200) reflection, indicated by arrows in Figure 3(a), is relatively high for all three films. This reflection was utilized to calculate f_a and, thus, f_c. It was found that the main-chain crystal orientation increases with the application of tension during annealing, other variables being equal. Figure 4 displays the f_c results for the A1 annealed films as a function of the tension level and annealing temperature for a fixed annealing time of 20 min. Although the measured change in f_c is small, it does systematically increase as the specific tension level is increased for a fixed annealing temperature. Additionally, the crystalline orientation becomes greater along the MD as the annealing temperature is increased for a fixed extension level, as long as the tension level is greater than zero.

The effect of annealing time in conjunction with the tension level on f_c is displayed in Figure 5 for the fixed annealing temperature of 205°C. It is recognized that with an increasing annealing time and increasing tension that f_c increases asymptotically, although the overall change in f_c is small. The trends in these results were qualitatively supported with IR dichroism measurements, as displayed in Figure 6, which is a plot of the dichroic ratio (D) for the 918-cm^{-1} band and is expressed as a function of the annealing time and level of tension. As the extension level increases, the dichroic ratio, which in this case is related to the overall sample orientation, asymptotically increases for a fixed annealing temperature (205°C) and a fixed annealing time. Further, as the annealing time increases from 5 to 20 min, the dichroic ratio increases as did f_c, as obtained by the WAXS results presented previously in Figure 5. An example of the parallel and perpendicular FTIR absorption spectra for the PMP films is shown in Figure 7, which is of the A1 precursor. A fact not yet addressed that arises from Figures 3–6 is that for the *free-annealed* specimens the crystalline orientation is *not affected* by the annealing time or temperature. In summary, the orientation results presented in Figures 3–6 were representative for all the films prepared from all resins.

The film morphology was also influenced by the annealing variables as observed in the bulk with TEM after RuO_4 staining as well as on the film surface with AFM. Figure 8(a–c) depicts AFM micrographs of A1 films annealed at 180, 205, and 215°C, respectively, for 20 min. Based upon the

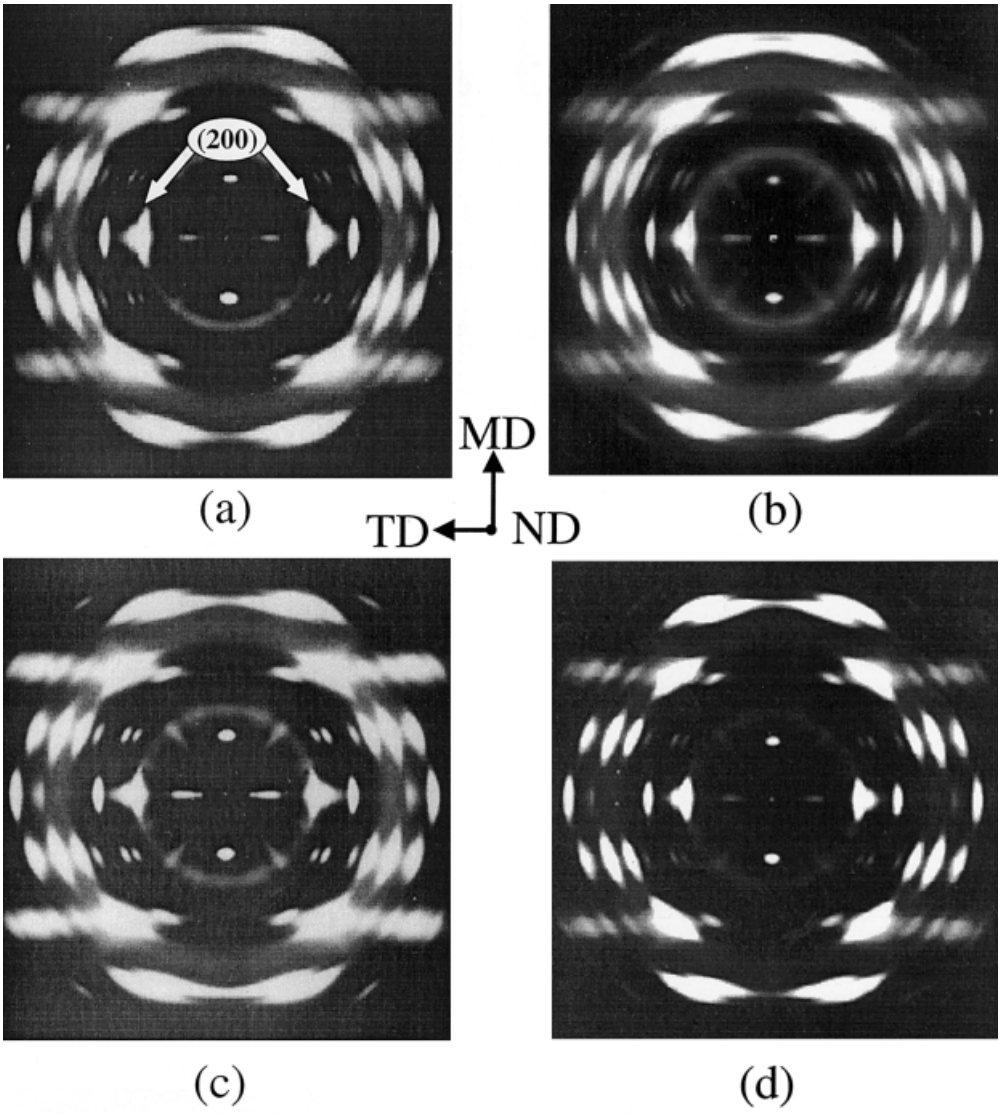

Figure 3 WAXS photographs of A1 films: (a) precursor; (b) free-annealed at T_a = 205°C for t_a = 20 min; (c) 3% tension T_a = 205°C for t_a = 20 min; (d) 15% tension T_a = 205° for t_a = 20 min. MD direction shown.

morphological analysis of these free-annealed films, it is observed that the stacked lamellar morphology remains intact for the A1 films annealed at 180°C [Fig. 8(a)] and 205°C [Fig. 8(b)]. However, the A1 film annealed at 215°C [Fig. 8(c)] has undergone some morphological change. This change appears to be some loss of the well-stacked lamellar structure, suggesting surface or larger-scale melting. Such large-scale melting of the film would not be beneficial for later lamellar separation upon uniaxial deformation in the final stage, and, thus, annealing temperatures were limited to a maximum of 205°C for the main study.

The effect of tension (percent extension) during annealing on the surface morphology is displayed in Figure 9(a–b) for the A1 films annealed at 205°C for 20 min. The free-annealed specimen corresponding to these conditions was previously presented in Figure 8(b). From these micrographs, it is apparent that, with increasing extension, lamellar deformation increases. In fact, some distinct lamellar separation has taken place, albeit to a limited extent, at a level of 15% tension [Fig. 9(b)], thus creating small surface voids on the order of nanometers (i.e., nanovoids). These are in contrast to the microvoids produced during the later stretching stage. Upon removal

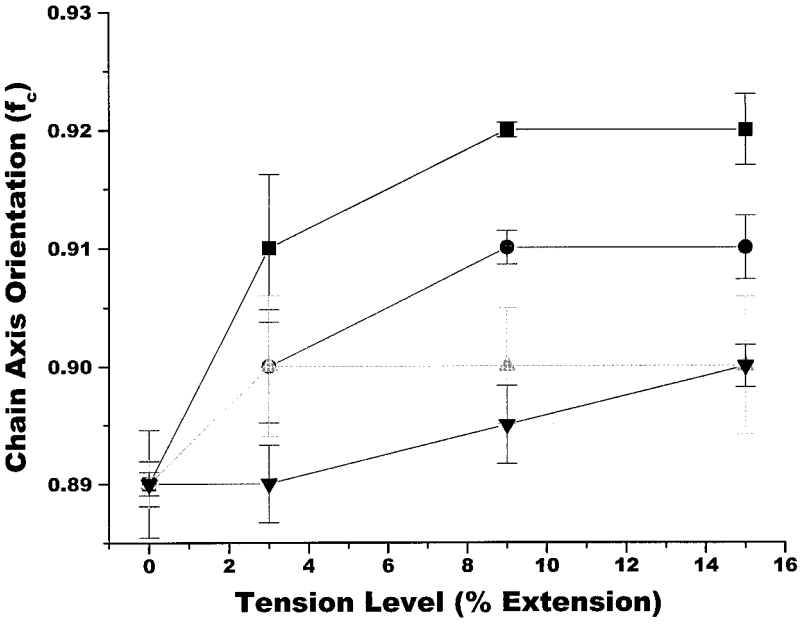

Figure 4 Main-chain orientation (f_c) of the A1 film's dependence upon annealing tension level and T_a for a t_a of 20 min: (-■-) T_a = 205°C; (-●-) T_a 180°C; (-▲-) T_a = 160°C; (-▼-) T_a = 145°C.

of the sample from the annealing oven, those films under tension displayed an observable increase in whitening (haze) that increased with the tension level. This is consistent with the AFM findings. The voids induced by tension increase the number of interfaces within the film, and, as a result, a greater fraction of the incident light is scattered and/or reflected. The AFM technique

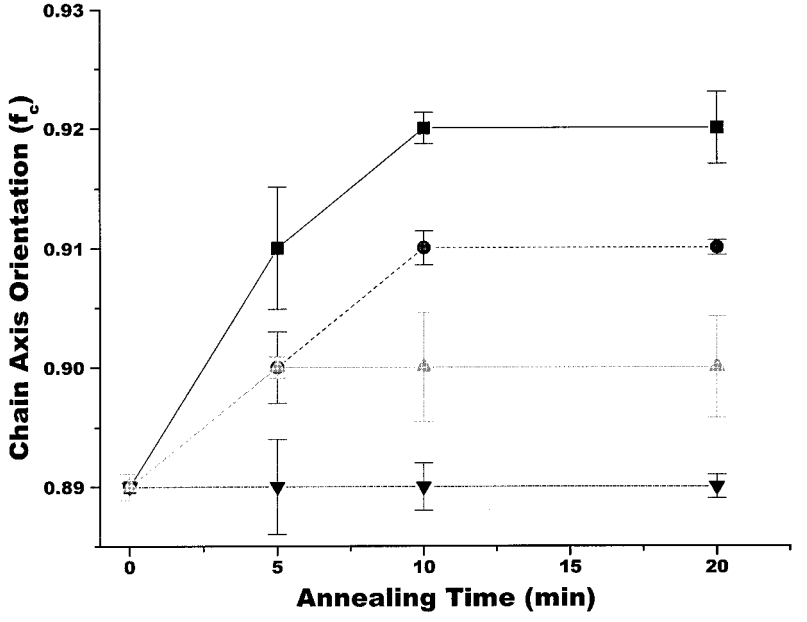

Figure 5 Main-chain orientation (f_c) of the A1 film's dependence upon annealing tension level and t_a for a T_a of 205°C: (-■-) 15% tension; (-●-) 9% tension; (-▲-) 3% tension; (-▼-) free-annealed (0% tension).

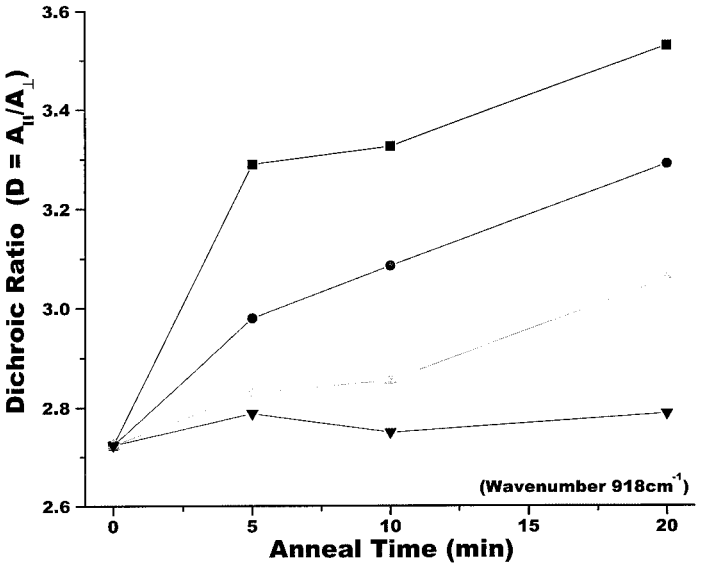

Figure 6 Dichroic ratio (D) for the A1 film's dependence upon annealing tension level and t_a for a T_a of 205°C using the 918-cm^{-1} band: (-■-) 15% tension; (-●-) 9% tension; (-▲-) 3% tension; (-▼-) free-annealed (tension of 0%).

was utilized solely to analyze the surface morphology of the PMP films, and the bulk-film morphology may be different from that of the surface.

TEM was also performed on the annealed PMP films after staining with RuO_4. Two representative TEM micrographs of the annealed A1 films are displayed in Figure 10(a,b). These micrographs are from two of the same films displayed in Figure 9(a–c), that is, A1 films annealed at a temperature of 205°C for 20 min using 9 and 15% extension, respectively. It is evident upon examination of these TEM micrographs that the lamellae become somewhat deformed as the extension level during annealing increases. These findings validate the AFM surface results and further suggest that there is no difference between the bulk and surface morphology. This is not surprising since a previous HDPE[2] investigation noted that there is no difference between the surface and bulk morphologies, where those samples were also extruded to a film thickness of about 1 mil.

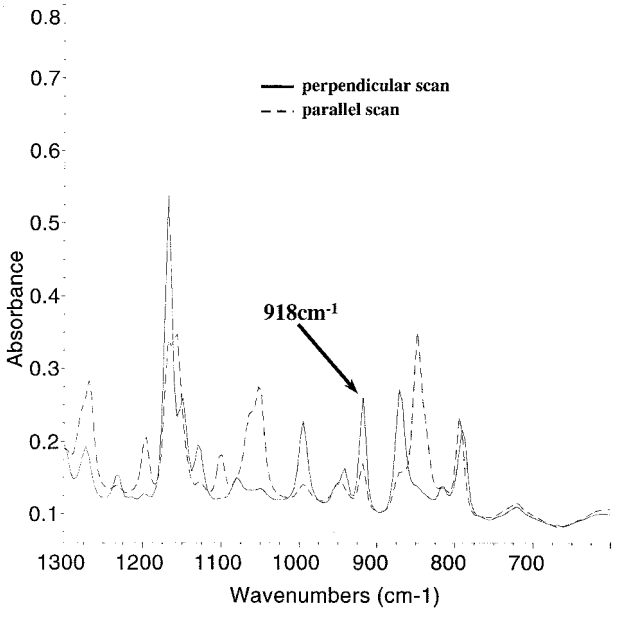

Figure 7 FTIR spectra of the parallel and perpendicular scans for the 918- cm^{-1} band obtained on the A1 precursor.

For all the A1 films, the effect of the tension level during annealing had no apparent consequence on the level of crystallinity or the crystalline melting point for a constant annealing temperature and time. In contrast, both annealing temperature and time did influence these same two properties. The melt temperature appears to be slightly enhanced by the annealing temperature and time as shown in Table III. These results are for selected samples, where the reader will note the measured lack of influence tension has on either film property (T_m or X_c) versus the effect of the annealing temperature and time.

Similar results are shown in Figure 11, where the full DSC scans are displayed for three specific

A1 films. A rather sharp melting peak characterizes each scan, including the precursor. The melting peak of each annealed film has shifted by approximately the same amount, regardless of tension level. In this figure, each annealed film presented had utilized a temperature of 205°C for 20 min. The remainder of the annealing results for the resin A and resin C films were comparatively similar to those presented. Both the crystallinity and melting point of the resin B films were not determined for the annealed films. This was due to the presence of multiple melting peaks upon annealing, as can be observed in Figure 12, where the multiple melting peaks are likely a consequence of the higher comonomer content present in resin B (ca. 6.5 wt %). In this figure, the DSC heating traces of three B1 films are presented: the precursor, a free-annealed film, and a film annealed under 15% tension where the two latter films were annealed at 205°C for 20 min.

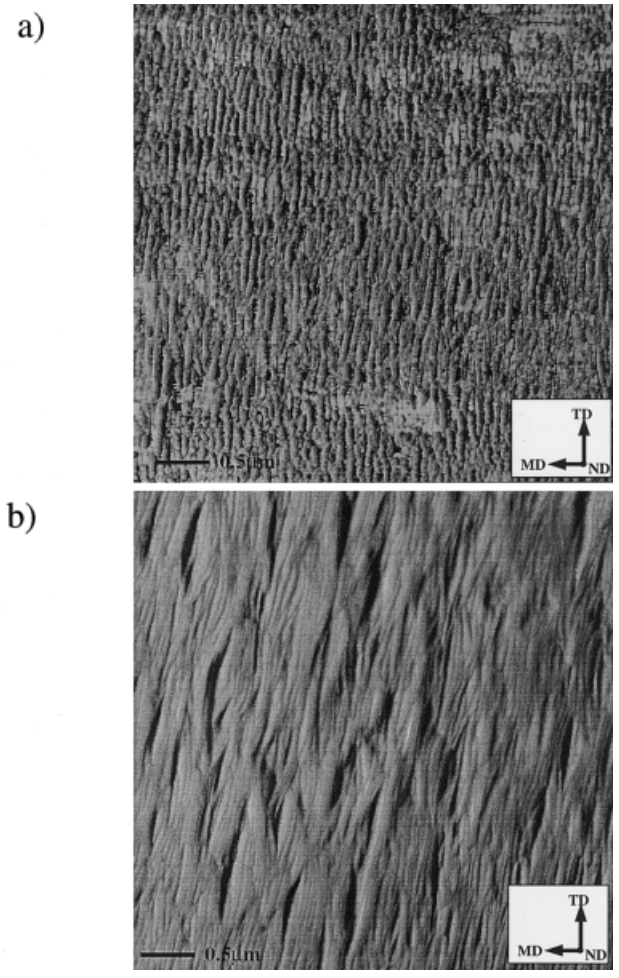

Figure 8 AFM phase images of the A1 free-annealed films with t_a = 20 min: (a) T_a = 205°C; (b) T_a = 215°C. The MD is labeled. The images are 3 × 3 μm.

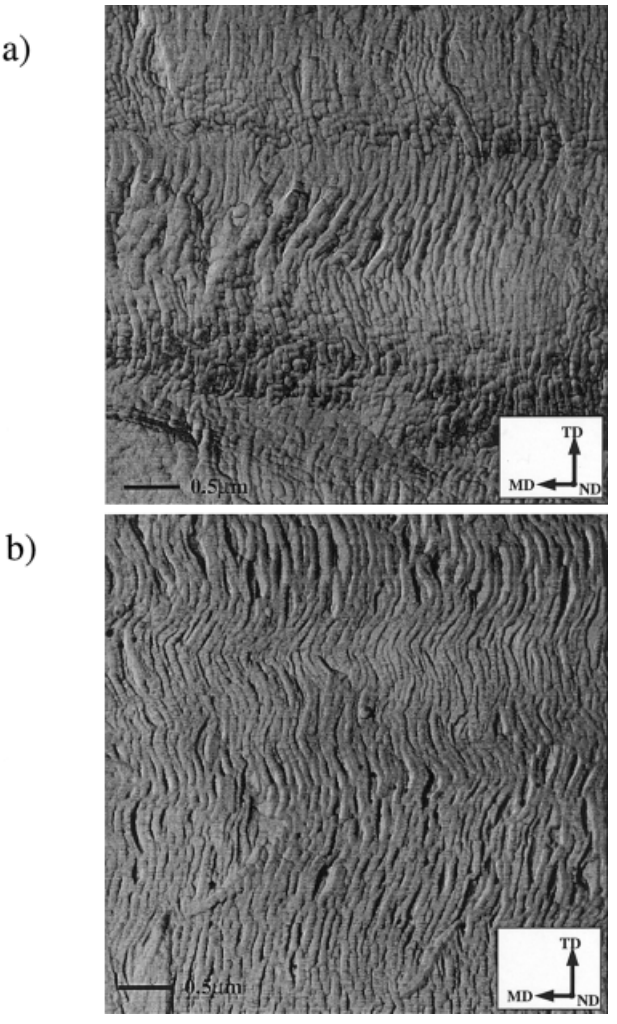

Figure 9 AFM phase images displaying the influence of tension during annealing on the morphologies of selected A1 films where T_a = 205°C and t_a = 20 min: (a) 9% tension; (b) 15% tension. The MD is labeled. The images are 3 × 3 μm.

The annealing temperature and time have also been observed to affect the relaxation attributed to crystalline mobility (α_c relaxation).[10,16,26] In the case of our PMP films, the magnitude of the overall relaxation decreased as a function of the crystallinity. This behavior is displayed for three A1 films, including the precursor, in Figure 13. Additionally, it was recognized that as the crystallinity increases the temperature associated with the maximum in the α_c relaxation (termed $T_{\alpha c}$) shifted to higher values. In contrast, the relaxation associated with cooperative segmental mobility (T_g relaxation) decreased in overall mag-

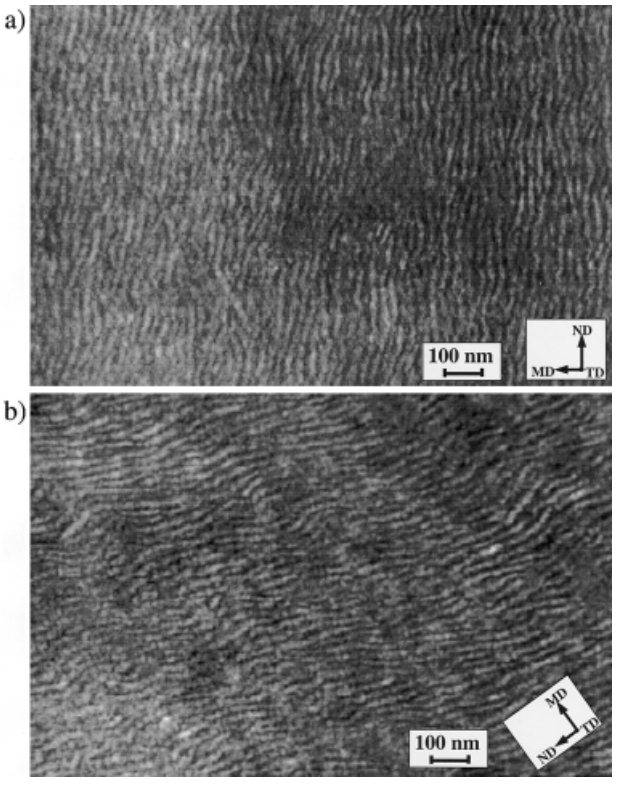

Figure 10 TEM micrographs of RuQ_4-stained A1 annealed films where t_a = 205°C and T_a = 20 min: (a) 9% tension; (b) 15% tension. The MD is shown.

nitude for the film annealed at the higher temperature (205°C) as a result of the higher crystallinity. For the film annealed at 160°C for 20 min, a small crystallinity increase occurred, but the T_g relaxation remained constant as shown in Figure 14. The effect of tension did not appear to systematically alter the overall magnitudes of either the α_c or T_g relaxations or the temperatures associated with the maximum in the PMP relaxations. These findings are in contrast to a report[27] which determined that the uniaxial draw ratio influenced the PMP relaxations, where in that investigation a maximum draw ratio of 6 was utilized. Thus, the lack of a systematic effect observed in our case is likely the consequence of the low tension levels utilized. The α_c and T_g relaxations of the resin C films were comparable to those of resin A with respect to both changes in magnitude and $T_{\alpha c}$ with the crystallinity. As was previously shown, the mechanical relaxations of the resin B films did not systematically change and were also difficult to analyze due to the convoluted nature of the α_c and T_g relaxations. Thus, no DMS data are presented regarding this resin. It will be shown in the next section, which addresses the stretching results, that the convoluted α_c relaxation characterizing the resin B films has adverse consequences on the formation of microporous membranes.

Microporous Development by Stretching (Stage Three)

The annealed films were subjected to the two-step stretching procedure described earlier. The actual stretching apparatus employed produced only uniaxial extension and, thus, the lateral dimensions are not constrained. Besides the crosshead speed, which was kept constant throughout the entire study at 150 mm/min, the variables of temperature and extension level were considered for each step. The cold-stretch temperatures studied were 40 [approximately equal to the PMP T_g (ref. 28)], 70, 80, and 90°C with extension levels (% CS) equal to 50, 65, 80, and 90%. The hot-stretching temperatures utilized were 120, 160, and 180°C, while the levels of extension (% HS) were 50, 65, 80, and 90%. The levels of extension were calculated using eq. (4):

$$\% \text{ Extension} = \frac{l_f - l_0}{l_0} \times 100\% \qquad (4)$$

where l_f is the final length of the film after the cold- or hot-stretch step, while l_0 is the initial length of the film *prior to any cold stretching*.

Table III Pertinent Film Characteristics of Selected A1 Annealed Films

~0.89	~0.89					
T_a (°C)	160	205	205	205	205	205
t_a (min)	20	10	20	20	20	20
% Tension	Free	Free	Free	3	9	15
T_m (°C)	230	230	233	232	232	233
X_c (%)	65	67	71	69	70	71
f_c	~0.89	~0.89	~0.89	0.91	0.92	0.92

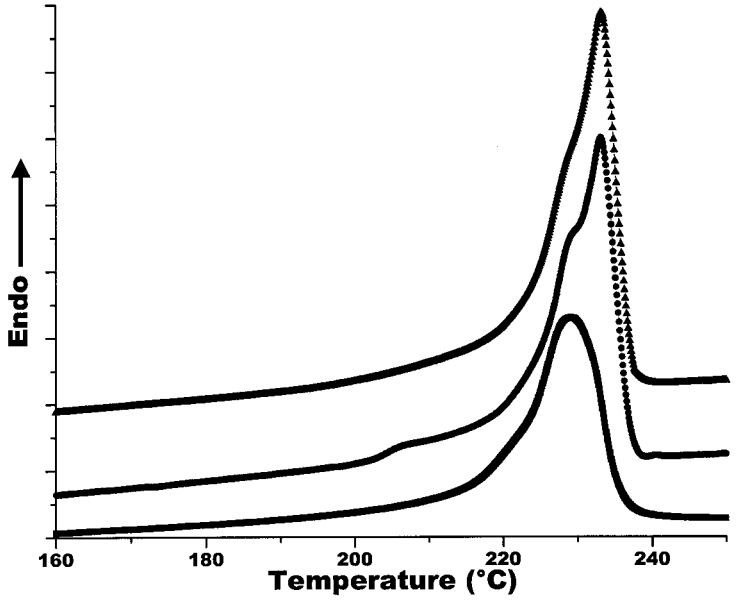

Figure 11 DSC heating scans of the A1 precursor and annealed films (T_a = 205°C for t_a = 20 min): (-■-) precursor, (-●-) free-annealed, and (-▲-) 15% tension utilizing a heating rate of 30°C/min.

Immediately after the hot-stretching step, a relaxation/heat-setting step was employed in the MEAUS process. In this study, the relaxation/heat-setting step occurs at the same temperature as does hot stretching, where relaxation amounts equal to 0, 20, and 40% were investigated while the heat-setting time was held constant at 10 min.

From the above, it clear that the possible number of annealing/stretching combinations is large, but the authors do not want to give the impression that every combination was attempted. In-

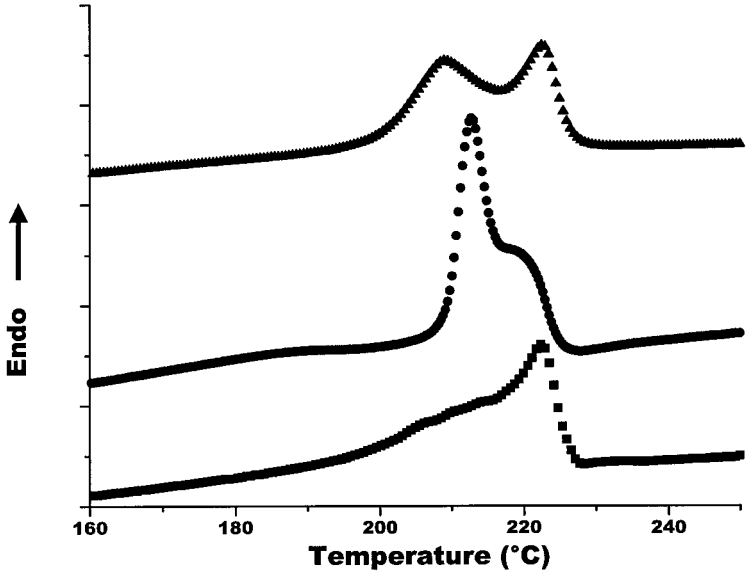

Figure 12 DSC heating scans of the B1 precursor and annealed films (T_a = 205°C for t_a = 20 min): (-■-) precursor, (-●-) free-annealed, and (-▲-) 15% tension utilizing a heating rate of 30°C/min.

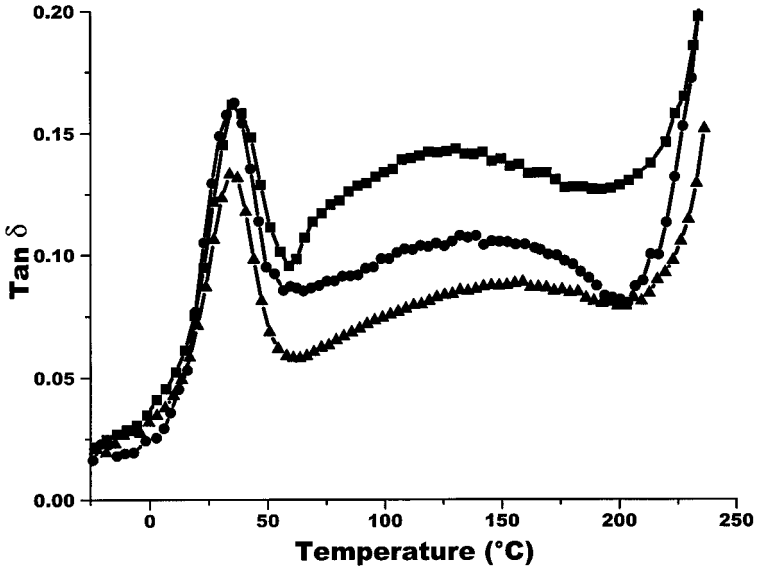

Figure 13 Tan δ as a function of temperature for the A1 precursor and annealed films (t_a = 20 min): (-■-) precursor,; (-●-) T_a = 160°C; (-▲-) T_a = 205°C. These data were obtained utilizing a heating rate of 2°C/min and a frequency of 1.0 Hz.

stead, the samples reported here will represent the general findings and will be based on a standard set of annealing and stretching conditions. The standard annealing/stretching variable combination, hereafter referred to as the *standard condition*, consists of a precursor that is free-annealed at a temperature equal to 205°C for 20 min, followed by cold stretching at 70°C to 50% extension, then hot stretching at 160°C to 90% extension without any relaxation (0%). A nomenclature for designating the final film histroy is employed, which utilizes the starting precursor

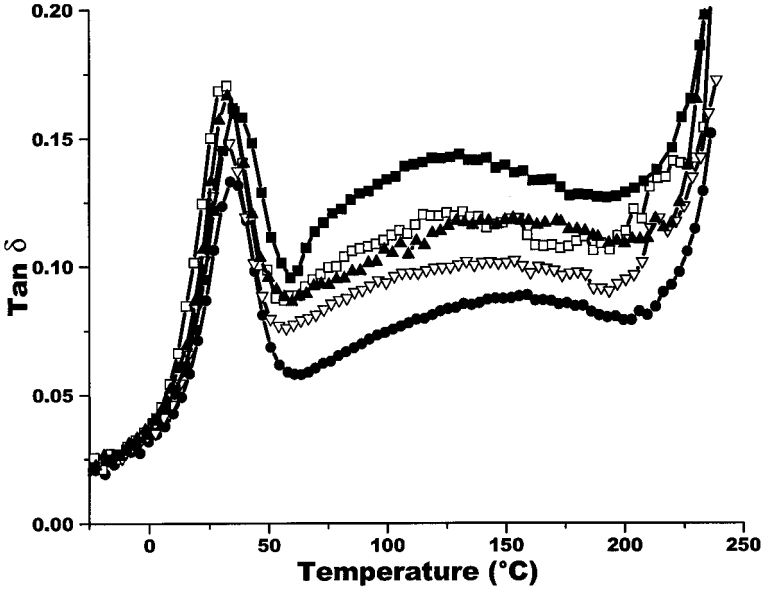

Figure 14 Tan δ as a function of temperature for the A1 precursor and annealed films (T_a = 205°C and t_a = 20 min): (-■-) precursor; (-●-) free-annealed; (-squ;-) 3% tension; (-▲-) 9% tension; (-▽-) 15% tension. These data were obtained utilizing a heating rate of 2°C/min and a frequency of 1.0 Hz.

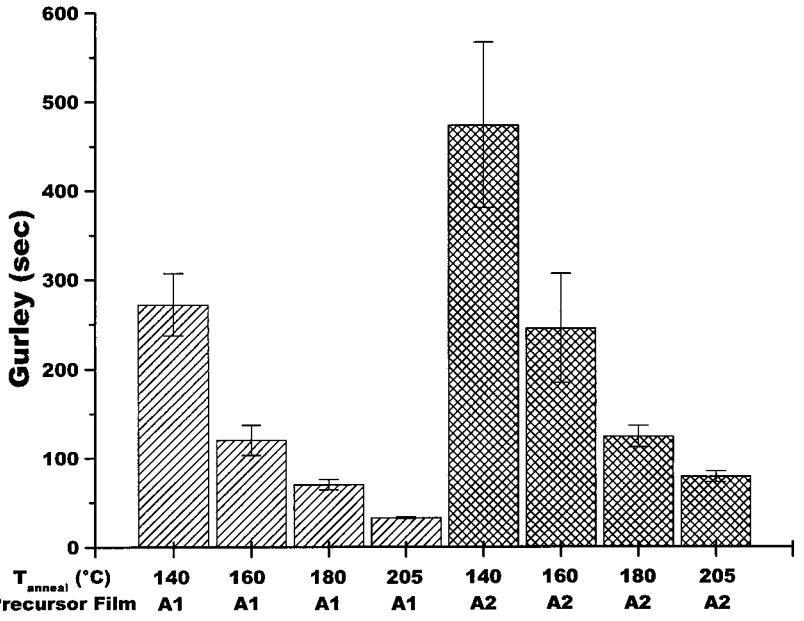

Figure 15 Effect of annealing temperature on the Gurley number of A1 and A2 stretched films with the remainder of the main annealing/stretching condition kept intact.

label along with any annealing and/or stretching variable that was altered from the standard condition. For example, if an annealed A1 film was cold-stretched at a temperature equal to 40°C instead of 70°C, the final stretched sample would be labeled A1-T_{cs}40. It would be assumed that the other annealing and stretching conditions were analogous to the standard variable combination.

In this section, numerous process variable combinations will be presented with regard to their influence on final film morphology and permeability (inverse function of Gurley number). These combinations will include the melt-extruded precursor morphology and f_c value; the annealing temperature, time, and tension level (percent extension); the cold-stretch temperature and percent extension; as well as the hot-stretch temperature and percent extension. The resin A precursor films A1 and A2 were utilized mainly to investigate the effects of these variable combinations and, thus, the forthcoming results will focus largely upon these materials. Extensive annealing and stretching variable combinations were also employed on the resin B and C films. Selected results from these latter studies will be addressed following those of resin A.

The effect of the annealing variables on the membrane permeability and morphology will be presented first. In Figure 15, the Gurley number dependence on the annealing temperature for the stretched films from precursors A1 and A2 is shown. Recall that other than the annealing temperature the remainder of the standard annealing/stretching condition was kept constant for the stretched films presented in this figure. It is observed that the Gurley number decreased with an increasing annealing temperature for both the resin A films A1 and A2. Additionally, note that the A1 stretched films possessed lower average Gurley numbers than that of the comparable A2 stretched films, that is, those films annealed and stretched at similar conditions. The reader may recall that the precursor A1 had an f_c of 0.89 while that of the precursor A2 was 0.83. This latter result suggests that membrane permeability also increased with a higher crystal orientation. While not presented here, when equivalent stretching conditions were used, it was found that film rupture during stretching occurred more frequently for films annealed at a lower temperature compared with films annealed at a higher temperature. Further, the annealing time played an important role in the frequency of film rupture during stretching. Specifically, the shorter the annealing time, the more often the film broke during stretching.

The annealing time also influenced the membrane permeability, as shown in Figure 16, where

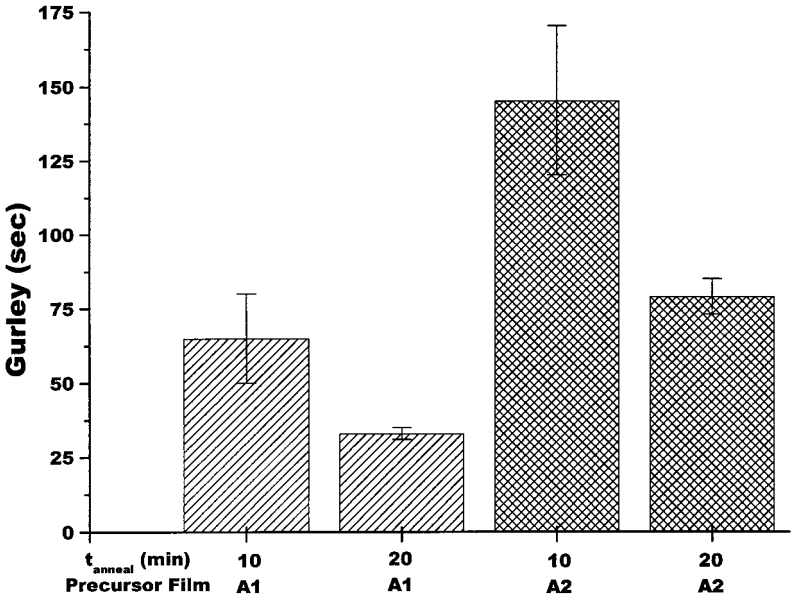

Figure 16 Effect of annealing time on the Gurley number of A1 and A2 stretched films with the remainder of the main annealing/stretching condition kept intact.

the Gurley number dependence on annealing times of either 10 or 20 min for A1 and A2 stretched films is displayed. In this figure, it is seen that the Gurley number is higher for either stretched A1 or A2 films annealed at the shorter of the two times. Data from experiments utilizing a 5-min annealing time, which are not displayed here, were found to produce permeable stretched films but with substantially higher Gurley numbers (lower permeability) than those of the final films annealed at either 10 or 20 min, all other variables remaining constant. It is noted that the A1 final film possesses a lower Gurley value than does the A2 stretched film for equal annealing/stretching conditions. For example, the Gurley number of the membrane A1-t_a20 equals 33 s, while that of A2-t_a20 equals 79 s. The reader may recall that Gurley numbers less than 100 s characterize a "quality" microporous film. Thus, Figure 16 indicates that three such membranes were achieved.

The remaining annealing variable, tension (percent extension), was shown earlier to influence the morphology of the annealed film; thus, it was to be expected to alter the microporosity and permeability of the final stretched film. Indeed, this is true, as observed in Figure 17, which displays the Gurley number as a function of the tension level during annealing for the films from precursors A1 and A2. In either case, it is recognized that with increasing tension the Gurley number increases. In fact, when a tension level of 15% was utilized, the Gurley number for either stretched film from A1 or A2 was equal to or greater than 1000 s, indicating an essentially impermeable film. The morphologies, as viewed with AFM, are shown in Figure 18(a–d) for selected A1 membranes, specifically, A1-%ext0 (standard condition), A1-%ext3, and A1-%ext9. There is detectable microporosity to varying degrees in these films. The finer structure of a PMP final film can be observed in Figure 18(d), which is an AFM micrograph of the same membrane shown in Figure 18(a), except at higher magnification. Note that the interlamellar fibers are oriented parallel to the MD and stretching direction or perpendicular to the lamellae. The stretched film morphologies of A1-%ext0 and A1-%ext3 [Fig. 18(a,b), respectively] are roughly identical and both possess relatively large microporous structures. The stretched films annealed under higher levels of tension, A1-%ext9 [Fig. 18(c)], display a deformed microporous morphology. The membrane A1-%ext15, not shown here, possessed little if any microporous character, explaining the reasoning behind its measured Gurley number of approximately 1000 s. To possess a low Gurley number, the microporosity must also occur throughout the *entire crosssection* of the stretched film, as is revealed via SEM in Figure 19. This figure is an SEM micrograph of the A1 membrane produced using the standard annealing/stretching condi-

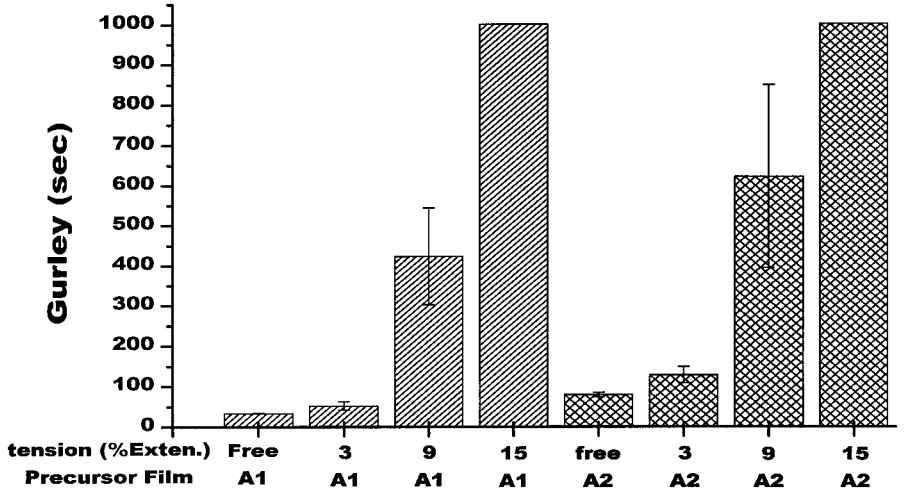

Figure 17 Effect of tension level during annealing on the Gurley number of A1 and A2 stretched films with the remainder of the main annealing/stretching condition kept intact.

tion, where the film is viewed along its transverse direction (TD), which is in contrast to the normal direction (ND) utilized for the AFM micrographs.

We now address the effect the cold-stretch parameters, T_{cs} and % CS, have on the final film microporous structure and permeability. Since we have established that the annealing/stretching results from precursor A2 parallel those from A1, except that a lower permeability is obtained for the A2 membranes, the remaining resin A data will only consider results from film A1. Figure 20 is a plot of the Gurley number as a function of the level of cold-stretch extension. Each plot also provides results for a constant value of the cold-stretch temperature. It is recognized that as the specific extension level was increased from 50 to 90% the membrane Gurley decreased. However, if the Gurley number was normalized by the final film thickness (not shown here), it would be observed that there is a slightly higher normalized Gurley for a film cold-stretched at 90% versus those stretched at either 65 or 80%. In fact, the local minima in a normalized Gurley would occur at an approximately 80% cold stretch. Upon further analysis of the data within Figure 20, it is discovered that the temperature of cold stretching also influences the Gurley number. Specifically, the Gurley number decreases when comparing an A1-T_{cs}40 stretched film to an equivalent A1-T_{cs}70 stretched film. However, upon increasing the cold-stretch temperature to 90°C, the Gurley number decreases. In fact, films produced using a cold-stretch temperature of 90°C possess the lowest permeability (largest Gurley) versus other films presented in that figure with similar % CS values. The morphology of the A1 stretched film A1-T_{cs}90, as obtained via AFM, is displayed in Figure 21. For comparison purposes, the reader will recall Figure 18(a)—the AFM micrograph of a membrane produced with the standard condition. In comparing these two films, it is evident that the final film A1-T_{cs}90 possesses a lower micropore concentration at the surface than that displayed in Figure 20(a). This finding aids in explaining the higher Gurley numbers (lower porosity) that occurred for films cold-stretched at 90°C versus the films that utilized lower cold-stretch temperatures. As an aside, the frequency of films breaking during stretching was higher as the cold-stretch temperature decreased, which is likely a consequence of a lower amorphous mobility as the this stretching temperature was decreased.

Gurley differences between A1 films of different cold-stretch extension levels occurred because the cold-stretch step acts to "nucleate" the micropores, whereas the hot-stretch step is utilized to increase or enlarge these structures. Thus, the more pore "nucleation" that transpires as a result of higher cold-stretch levels, the more uniform and numerous the micropores will be in the final film. Figure 22 displays an AFM micrograph of a microporous film, where the film was produced employing the standard annealing/stretching conditions but *without* the standard hot-stretch step. When it is compared with the film represented in

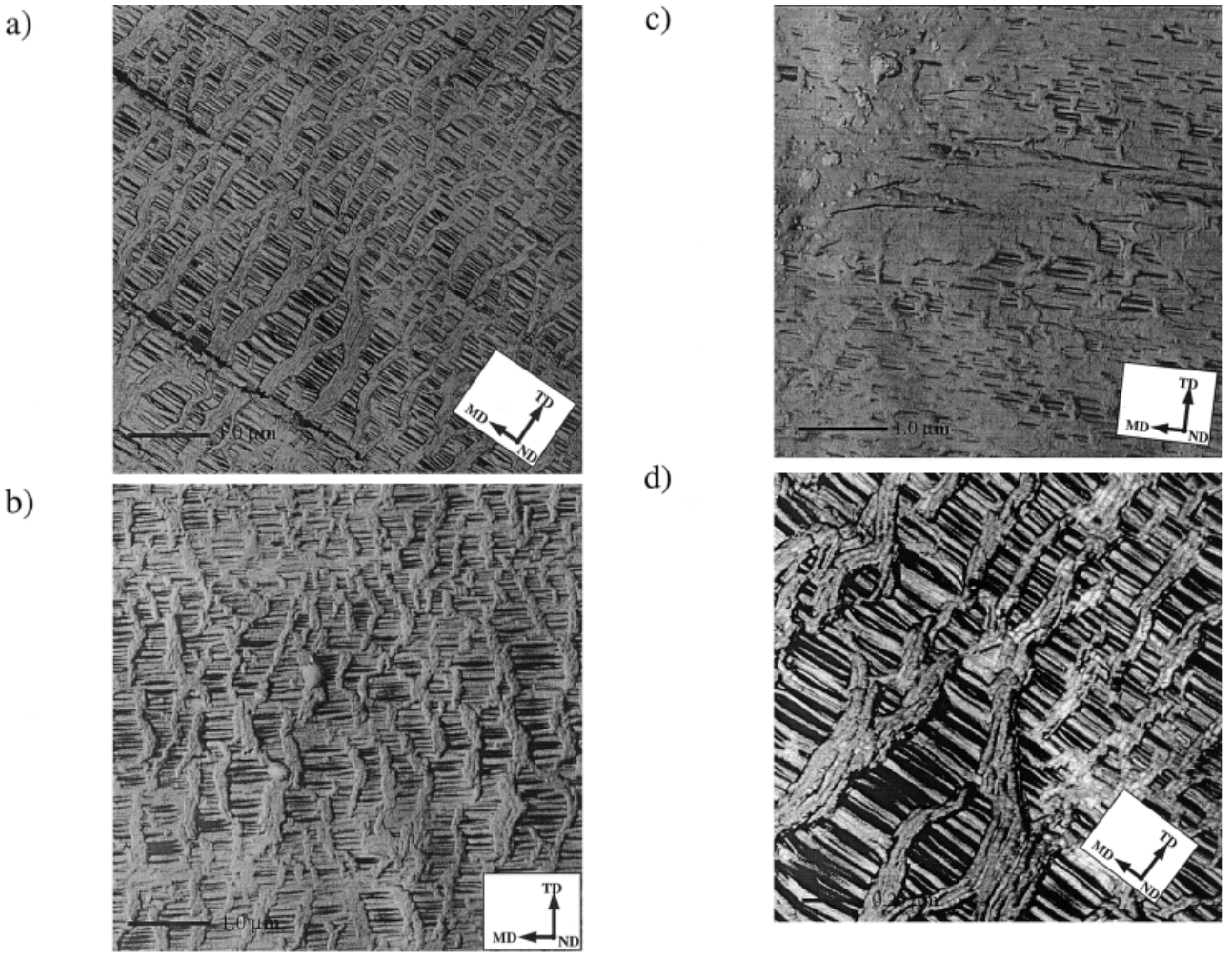

Figure 18 AFM images displaying the influence of annealing tension on stretched A1 membranes where T_a = 205°C and t_a = 20 min: (a) free; (b) 3% tension; (c) 9% tension; (d) free but at higher magnification than (a). The MD is labeled.

Figure 18(d), the above statement is essentially verified. The reader may recall that the final film presented in Figure 18(d) was produced utilizing the *entire* standard annealing/stretching condition.

Figure 23 is a plot indicating the dependence of the Gurley number on both the hot-stretch step parameters (T_{hs} and % HS). Based upon the AFM micrograph in Figure 22, which illustrates the effect of the hot-stretch condition on the morphology, it was expected that the Gurley number for these films should decrease with increasing hot-stretch extension. Indeed, as depicted in Figure 23, the Gurley number decreased as the specific extension level is increased. However, if the Gurley numbers were normalized on the membrane thickness, the film produced using the highest

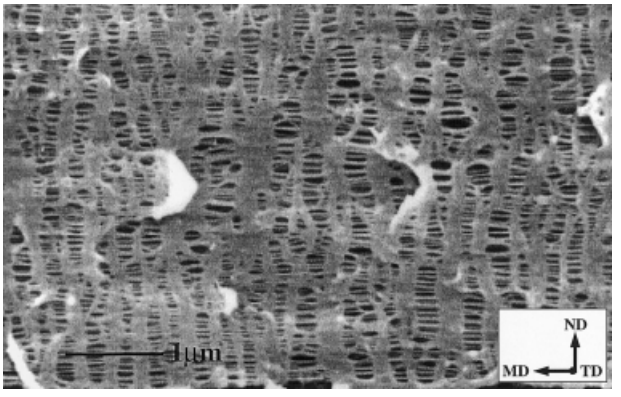

Figure 19 SEM micrograph of the cross section of the A1 membrane produced using the main annealing/stretching condition.

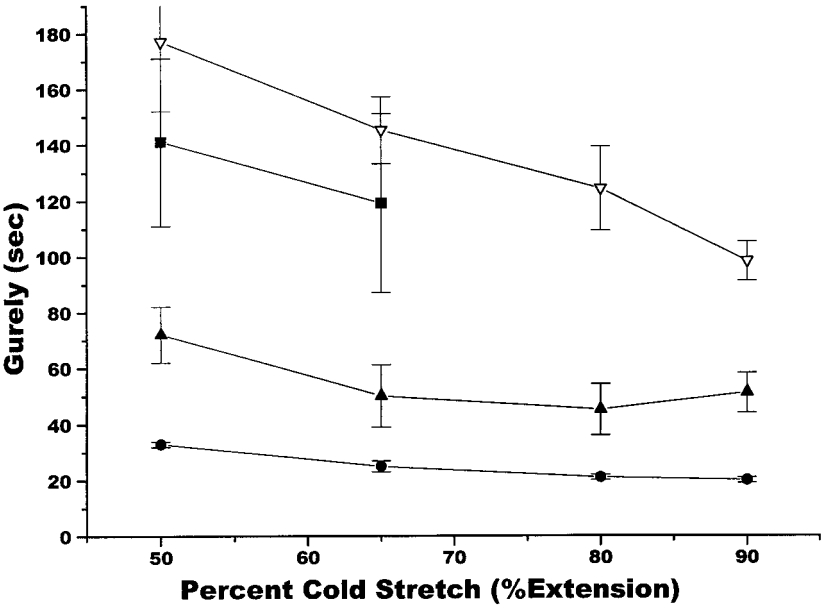

Figure 20 Effect of the cold-stretch parameters (T_{cs} and % CS) on the Gurley number for AL stretched films with the remainder of the main annealing/stretching condition kept intact: (-■-) T_{ca} = 40°C; (-●-) T_{ca} = 70°C; (-▲-) T_{ca} = 80°C; (-▽-) T_{ca} = 90°C.

level of hot-stretch extension (90%) possesses an equal if not a slightly higher normalized value versus the A1-% HS80 film. It is also observed in Figure 23 that the hot-stretch temperature, T_{hs}, influences the Gurley number. For a constant hot-stretch level, the Gurley number decreased as the specific hot-stretch temperature increased. This occurs regardless whether or not normalization of the Gurley number to film thickness was undertaken because for a constant total extension (i.e.,

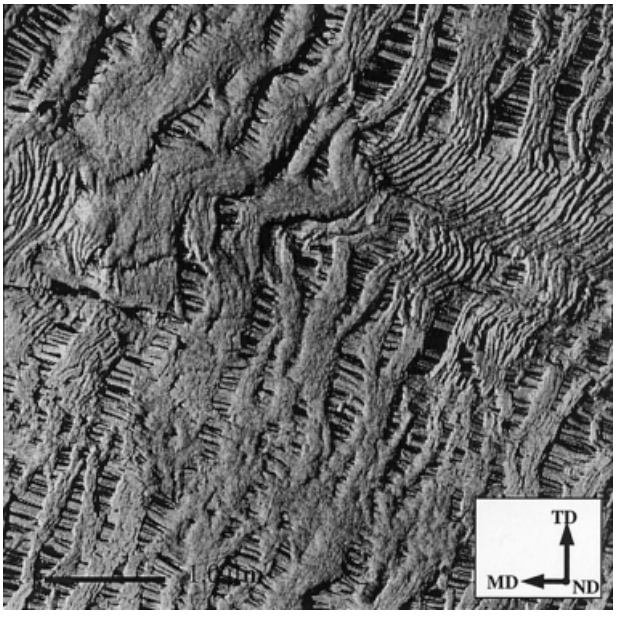

Figure 21 AFM image for the stretched membrane A1 with T_{cs} = 90°C. The MD is labeled. Images are 5 × 5 μm.

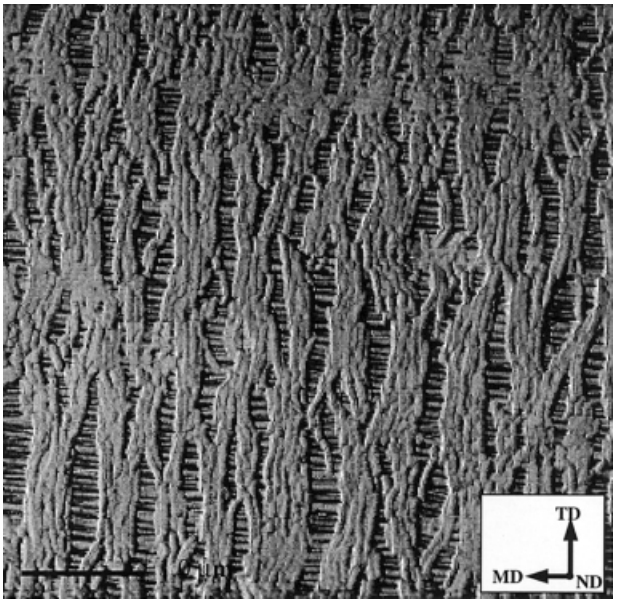

Figure 22 AFM image for an A1 stretched membrane where the hot-stretch step was not used. The MD is labeled. Images are 5 × 5 μm.

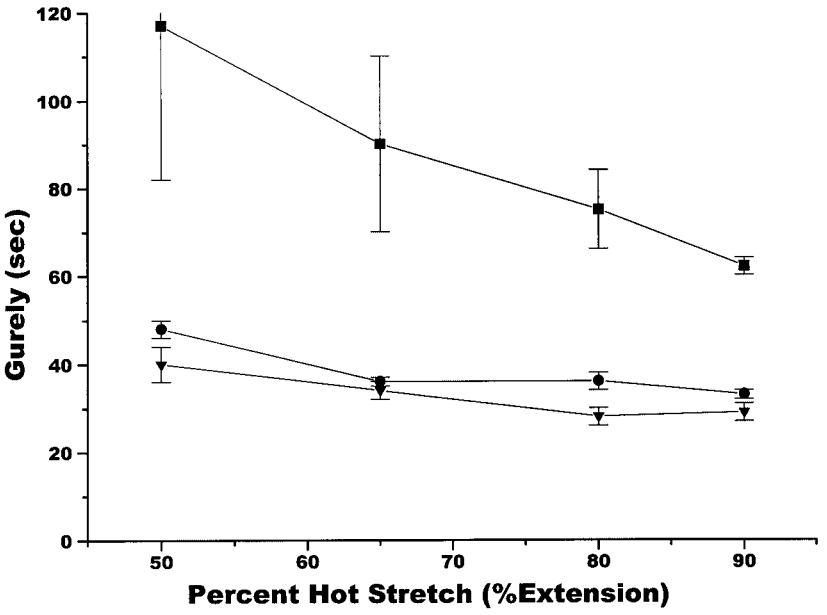

Figure 23 Effect of the hot-stretch parameters (T_{hs} and % HS) on the Gurley number for AL stretched films: (-■-) T_{ca} = 120°C, (-●-) T_{ca} = 160°C, and (-▲-) T_{ca} = 180°C, with the remainder of the main annealing/stretching condition kept intact.

% TS where % TS = % CS + % HS) the final film thickness was approximately the same.

If the effect of total percent stretch on the Gurley number was plotted, it would be similar to the behavior noted in either Figures. 20 or 23, because the reader only needs to sum the percent cold stretch with the percent hot stretch. In doing so, the total stretch values would be 100, 115, 130, and 140% extension for Figure 23 and 140, 155, 170, and 180% for Figure 20. The Gurley numbers corresponding to the stretched films with these % TS values are displayed in matrix form in Table IV along with stretched films possessing other % CS and % HS combinations (the % TS is provided at the top left corner). All the A1 stretched films displayed in this table possess Gurley numbers, which characterize these samples as being "quality" microporous membranes.

It was also recognized that if the percent total stretch remains constant, there does not appear to be any *significant* benefit to final film permeability if the percent cold stretch is larger than is the percent hot stretch within the total range of the stretching conditions studied. The effect of the total stretch on the final film morphology, as viewed with AFM, is shown for the two extreme cases of 100 and 180% in Figures 24(a,b), respectively. There is a slight observable difference in the micropore size between the 100 and 180% total stretch films, where the film produced using the larger total stretch is characterized by the larger micropore structure. Thus, the permeability difference between these films is accounted for. These results just presented are characteristics of membranes produced by annealing and stretching variable combinations, which did not utilize a relaxation step, that is, the relaxation

Table IV Gurley Numbers and the % TS (Top Number Each Set of Numbers) for A1 Membranes

% HS (% Extension)	% CS (% Extension)			
	50	65	80	90
50	100% 48 ± 5	115% 35 ± 3	130% 34 ± 2	140% 30 ± 2
65	115% 36 ± 2	130% 30 ± 2	145% 28 ± 3	155% 24 ± 1
80	130% 36 ± 2	145% 27 ± 1	160% 23 ± 2	170% 19 ± 2
90	140% 33 ± 1	155% 25 ± 2	170% 21 ± 1	180% 20 ± 1

These membranes were products of different % CS and % HS combinations. All other annealing/stretching parameters remained intact with the standard condition.

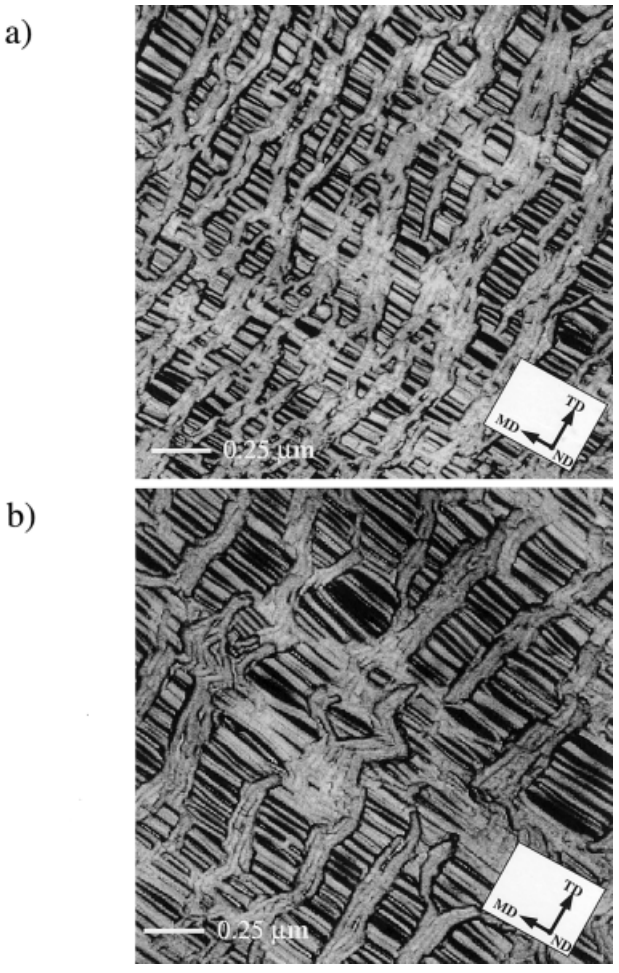

Figure 24 AFM height (left) and phase (right) images displaying the influence of total extension level (%TS) during stretching on A1 membrane morphology: a) %TS = 100% and b) %TS = 180%. The MD is labeled.

utilized was 0%. A relaxation step is, however, generally employed in the industrial process to allow the stretched films to partially recover (shrink) after finishing the hot-stretch step. The effect of such a relaxation step on the micropore structure and film permeability has been ignored in this report until now. In Figure 25, the Gurley number is displayed as a function of the percent relaxation (%rlx) for three A1 stretched films. One of these films, A1-%rlx0, was previously been presented as the stretched film utilizing the standard condition. The other films, A1-%rlx20 and A1-%rlx40, that utilize 20 and 40% relaxation, respectively, clearly indicate that by increasing the amount the film is allowed to relax the Gurley number increases. In fact, the stretched sample that was allowed to relax the most, A1-%rlx40, possessed a Gurley number of about 150 s, thereby indicating the lack of a "quality" microporous membrane. Within error, a nonquality Gurley number also characterizes the A1 membrane produced with 20% relaxation, A1-%rlx20.

In a similar manner to the resin A films, resin B and C films, B1 and C1, were annealed and subsequently stretched utilizing a number of the same variable combinations discussed. However, the results were dramatically different as are shown in Figure 25(a,b), respectively. In Figure 26(a), a typical AFM micrograph for a B1 final film is displayed. This film was produced with the standard annealing/stretching condition. It is clearly evident that this sample is absent of any microporous structure, and analogous results were observed for *all* other annealing and stretching variable combinations utilizing resin B precursors. Figure 25(b) also displays the lack of a microporous morphology. This AFM micrograph characterizes the stretched C1 film in which the standard stretching condition was also used. As with the resin B stretched films, the resin C films when stretched under an array of variable combinations were *all* devoid of a microporous structure; thus, no further results concerning the films of resins B and C will be presented here.

DISCUSSION

The annealing results presented clearly indicated that the physical properties of the film including the morphology, chain-axis crystal orientation (f_c), melting point (T_m), and the degree of crystallinity (X_c) can be controlled to varying degrees by the annealing temperature (T_a), annealing time (t_a), and the level of extension or tension. When uniaxial tension was applied during annealing, the morphology that resulted was the product of lamellar separation. This produced interlamellar voids on the order of nanometers in size, as viewed by AFM on the sample surface. Optically, the films annealed at higher tension levels possessed visibly more haze than did those annealed at lower tension levels. Regarding the TEM micrographs, the presence of micropores account for the increasing visible whitening or haze as the level of tension was increased. Similar TEM results were observed by Zhou and Wilkes for HDPE films when tension (extension) was applied, where the initial films also possessed well-defined stacked lamellar morphologies.[26] It was further reported that the main-chain orientation increased for the HDPE films with increasing de-

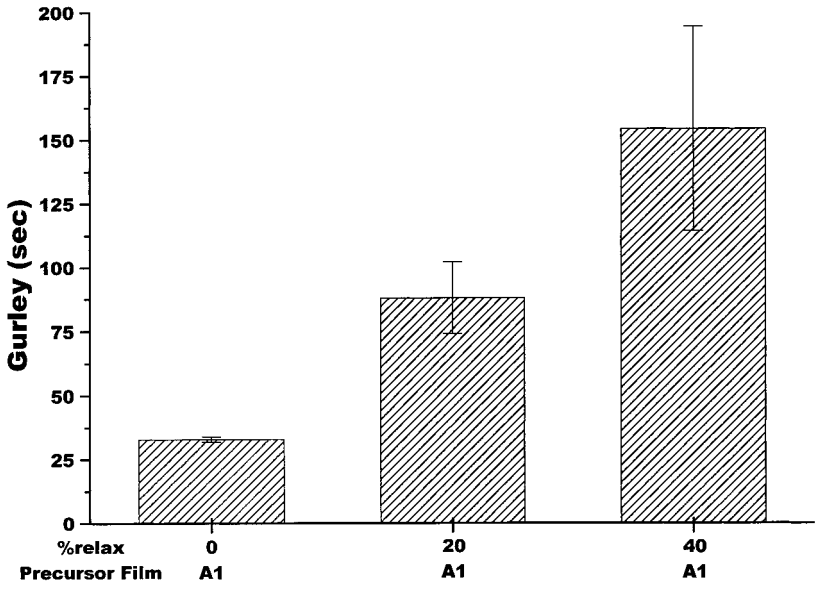

Figure 25 Effect of the percent the film is allowed to relax from the % TS after hot stretching on the Gurley number of A1 stretched films with the remainder of the main annealing/stretching condition kept intact.

formation during annealing. In our PMP films, as the annealing tension level was increased, the crystalline orientation also increased as expected. However, this annealing parameter did not affect the percent crystallinity (X_c) or the melting point (T_m) of our samples.

In the case of increasing the annealing temperature or time utilized, the annealed film crystallinity correspondingly increased. The melting temperature, however, was less influenced by these two annealing variables. Thus, the annealing temperature and time spent in the PMP α_c relaxation are two factors that distinctly influence the resulting crystallinity. The α_c relaxation for a given semicrystalline polymer is correlated to main-chain translational mobility within the crystalline phase, and thus given a sufficient temperature to activate this relaxation, redistribution of the tight folds, loose loops, and lengthening of the tie chains can occur according to some researchers.[11,14,16] These effects, according to Rault,[10] explain why annealing at elevated temperatures for longer times improves the rupture properties of semicrystalline materials that possess an α_c relaxation. Indeed, we reported that the frequency of film rupture decreased as the T_a or t_a utilized was increased, which was regardless of the stretching conditions.

The stretching conditions were shown to impact the final film properties such as the pore structure and permeability. The total amount of stretch was one such variable that influenced these properties. Greater overall film extension produced larger micropores (as was observed via AFM in Fig. 24), thus resulting in membranes of a lower Gurley number (higher permeability). Of the final films presented, the membrane possessing the lowest Gurley number was attained utilizing the highest total stretch (180%).

We now discuss the influence of the cold-stretch temperature on the Gurley number and pore size. As shown in the results presented, this variable was found to influence the film permeability in that as this stretching temperature increased from 40 to 70°C the Gurley decreased. However, upon increasing the temperature above 70°C, the Gurley number increased. This result is also displayed below in Table V, where the Gurley number dependence on various cold- and hot-stretch temperature combinations is presented. The initial decrease in the Gurley number with an increasing cold-stretch temperature is a result of greater mobility within the amorphous phase rather than within the crystal phase. This is because at 40°C a difference of only 5°C exists between the cold-stretch temperature and the PMP glass transition of 35°C. The more limited amorphous mobility at 40°C also accounts for the greater frequency of film rupture during stretching relative to higher cold-stretch temperatures.

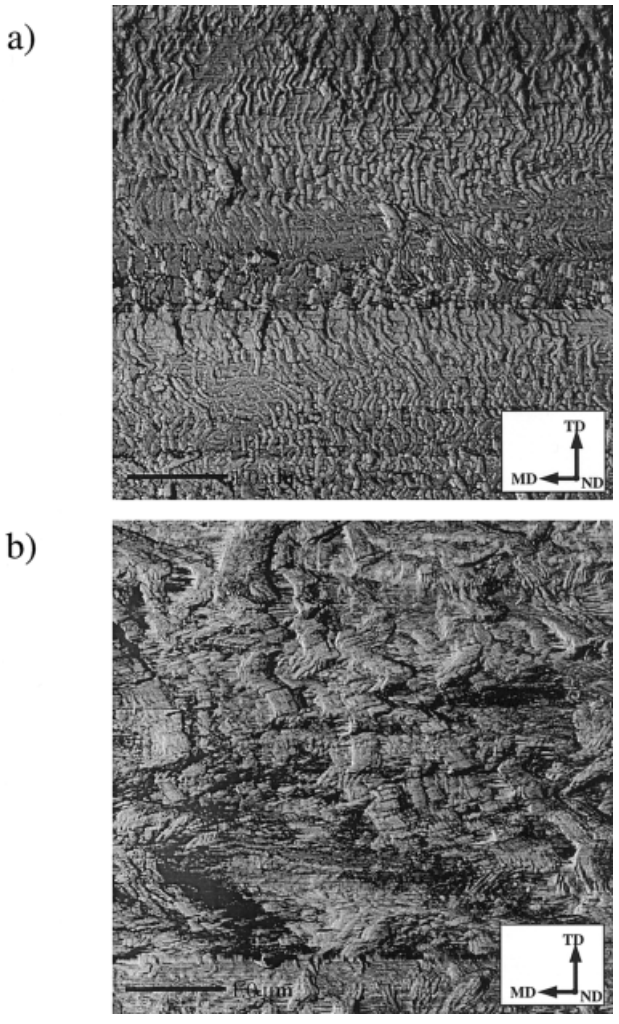

Figure 26 AFM phase images of the (a) B1 and (b) C1 stretched films produced utilizing the main annealing/stretching condition. The MD is labeled. Images are 5 $\times$ 5 μm.

However, upon stretching at the higher cold-stretch temperatures, the chain axes are able to translate through the crystal more readily as a result of greater activation of the α_c relaxation. The result is that at the lower cold-stretch temperature of 70°C the lamellae behave more solid-like (less chain slippage through the lamellae); therefore, greater micropore nucleation is possible, with the end result being more numerous micropores as was observable via AFM.

While chain slippage in the crystalline phase is not desirable for the cold-stretching step, it is exactly the desired outcome in the hot-stretching step. This results in greater lamellae separation as a consequence of higher levels of draw. As displayed in Table V, one notes that the Gurley number is the lowest for a hot-stretch temperature of 180°C. At lower hot-stretch temperatures, the Gurley values were not as low when compared with films hot-stretched at 180°C, all other MEUAS variables being equal.

From the above results, the porosity dependence on the annealing and stretching parameters was obtained. For the conditions analyzed, the highest membrane permeability for the resin A films was achieved utilizing an annealing temperature of 205°C for 20 min without tension (free-annealed) followed by cold stretching the film at 70°C and hot stretching at 180°C. Previously, however, the dependence of the cold-stretch extension level was based on a hot-stretch temperature of 160°C instead of 180°C—recall Figure 20. In Figure 27, the Gurley number as a function of the percent cold stretch is displayed, where the data presented in this figure are based on a hot-stretch temperature of 180°C. As expected, the absolute lowest Gurley number of 16 s occurs for the sample possessing the highest total stretch (180%). Upon normalization of the Gurley numbers to the final film thickness, as displayed in Table VI, it is noted that the lowest normalized value was achieved with a percent cold stretch of 80% and thus a total stretch of 170%. Therefore, for the resin A films, the optimum annealing/stretching condition utilizes a film that is free-annealed at 205°C for 20 min followed by cold stretching at 70°C to 80% extension and then hot stretching at 180°C to 90%. This, however, is without the implementation of a relaxation step after the hot-stretching step, as it was found that

Table V Effect of Different T_{cs} and T_{hs} Combinations on the Resulting A1 Microporous Film Gurley Number—All Other Annealing/Stretching Parameters Remained Constant with the Standard Condition

	T_{cs} (°C)			
T_{hs} (°C)	40	70	80	90
120	NP[a]	62 ± 2s	88 ± 14s	NA[b]
160	141 ± 30s	33 ± 1s	66 ± 10s	177 ± 25s
180	86 ± 16s	29 ± 2s	34 ± 4 s	67 ± 12s

[a]NP denotes a sample that was not able to be produced because sample rupture occurred repeatedly for a number of attempts during cold stretching.

[b]NA denotes a variable combination that was not attempted.

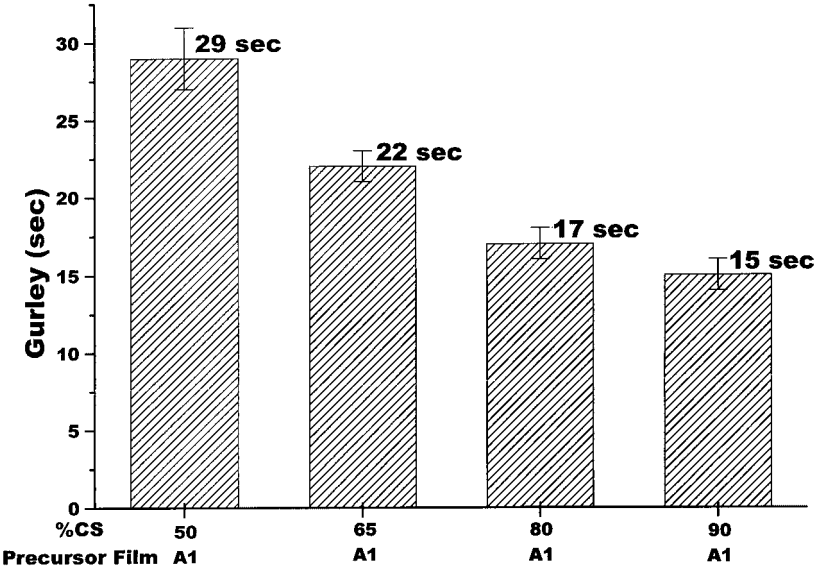

Figure 27 Gurley number dependence on cold-stretch extension level (% CS) for A1 stretched films using T_{ha} = 180°C, with the remainder of the main annealing/stretching condition kept intact.

the relaxation step decreases the pore size and, thus, the film permeability.

The effect the precursor f_c and morphology have on the stretched film permeability and structure has yet to be discussed. It was discovered that the precursor A1, when annealed and stretched at similar conditions to the A2 sample, possessed a higher permeability. It is reiterated that precursor A1 was characterized by a slightly more planar lamellar morphology and a higher f_c value with respect to the MD than that of the precursor A2. Therefore, the starting film morphology and orientation state play an integral role in the final film properties. In the vast majority of cases presented here, however, when annealed and stretched, resin A films were produced into microporous membranes.

The resin B or resin C films, however, did not form microporous morphologies when subjected to a large number of variable combinations identical to those applied to the resin A films. In the case of the resin B films, this result is attributed to its additional amount of the comonomer that adversely impacted its α_c relaxation. In the case of the resin C films, it is the precursor properties, specifically the morphology and f_c, that are believed to be the principal cause of poor microporosity. This conclusion regarding the resin C films is made since no other property with the exception of molecular weight was different from the resin A precursors. Additionally, the effect of f_c on the permeability has already been shown to be of consequence in the case of the resin A films. Recall that the resin A final film comparison took place between precursors possessing f_c values of 0.89 and 0.83, which is a relatively small difference that resulted in a detectable difference in permeability. The resin C film C1 is thus signifi-

Table VI Final A1 Film Gurley Numbers, Film Thickness, and Normalized Gurley Numbers as a Function of the % CS—All Other Annealing/Stretching Parameters Remained Constant With the Standard Condition

Sample	A1-%CS50	A1-%CS65	A1-%CS80	A1-%CS90
Gurley no. (s)	29 ± 2	22 ± 1	17 ± 1	16 ± 1
Film thickness (mil)	0.64	0.60	0.58	0.54
Normalized Gurley no. (s/mil)	45	37	29	30

cantly lower at 0.67—note that this was the highest f_c value measured for any of the resin C precursors.

From the above results and discussion, it was evident that the annealing and stretching parameters studied here impacted the final film microporosity. Furthermore, it is suggested by the authors that the criteria or prerequisites a semicrystalline polymer must be able to fulfill in order to form a "quality" microporous membrane via the three stage MEAUS process are as follows:

1. "Fast" crystallization kinetics;
2. A highly planar lamellae morphology for the extruded precursor;
3. "High" orientation of the crystalline phase in the precursor;
4. Proper film thickness (1 mil) and quenching rate to facilitate rapid heat transfer of the film;
5. Presence of an α_c relaxation.

CONCLUSIONS

The annealing and uniaxial-stretching behavior of melt-extruded precursor films from three resins were studied where each film was characterized as possessing a stacked lamellar morphology. The end goal was to produce microporous films from these precursors by applying the appropriate conditions.

It was recognized that with increasing annealing temperature or annealing time, the crystallinity was increased while the melting point was not significantly affected. The morphology was observably affected only for annealing temperatures equal to or above 215°C applied for 20 min. The application of tension during annealing also influenced the annealed film morphology. Lamellar separation was specifically found to occur by AFM and TEM. Further, a higher tension level during annealing produced an increase in the crystalline orientation.

The initial melt-extruded morphology and crystal orientation were found to be influential on the microporosity and permeability of the final film. In fact, a lower orientation value and slightly twisted lamellar morphology was believed to be the main reason why the precursors from resin C were not able to form microporous membranes. Morphological alterations resulting from annealing with and without tension were also found to influence the microporosity. Annealing time and temperature were critical as well not only to the final film but also in minimizing the frequency of film rupture during stretching. Specifically, films annealed at lower temperatures for shorter times ruptured more often during stretching than did films annealed at higher temperatures and longer times. This annealing effect on the film breakage for the PMP films was attributable to the presence of an α_c relaxation in the resin A films. This same relaxation was also used to account for other morphological effects that impacted the porosity. In the case of the resin B films, the comonomer may have affected the α_c relaxation in such a manner that was detrimental to the formation of microporous films via the MEAUS process.

The authors would like to thank the Celgard Corp. LLC for their continuing financial assistance for this project as well as the informative discussions that have taken place with them. The authors also thank Stephen McCartney for aiding in the TEM as well as the AFM instruction.

REFERENCES

1. Cannon, S. L., McKenna, G. B., Statton, W. O. Macromol Rev 1976, 11, 209.
2. Yu, T. H., Wilkes, G. L. Polymer 1996, 37, 4675; Erattum 1997, 38, 1503; J Rheol 1996, 40, 1079.
3. Yu, T. H., Ph.D. Dissertation (advisor: G. L. Wilkes), Virginia Tech, 1995.
4. Kamo, J., Uchida, M., Hirai, T. Jpn. Patent 63[1988]-256 712, 1988.
5. Noether, H. D. U.S. Patent 3 513 110, May 19, 1970 (to Celanese Research Group).
6. Gore, R. W. U.S. Patent 39 621 253, 1967.
7. Knobloch, R. W., Statton, W. O. U.S. Patent 3 299 171, Jan. 17, 1967 (to E. I. Dupont Denemours and Co., Inc.).
8. Johnson, M. B., Wilkes, G. L., submitted for publication in J Appl Polym Sci.
9. Druin, M. L., Loft, J. T., Plovan, S. G. U.S. Patent 3 801 404, 1974 (to Celanese Corp.).
10. Rault, J. JMS-Rev Macromol Chem Phys C 1997, 37, 335.
11. Popli, R., Mandelkern, L., Benson, R. S. J Polym Sci Polym Phys Ed 1984, 5, 407.
12. Boyd, R. H. Polymer 1985, 26, 323.
13. Marand, H., Xu, J., Srinivas, S. Macromolecules 1998, 31, 8219.

14. Boyd, R. H. Polymer 1985, 26, 1123.
15. Nakayasu, H., Markovitz, H., Plazek, D. J. Trans Soc Rheol 1961, 5, 261.
16. McCrum, N. G., Read, B. E., Williams, G. Anelastic and Dielectric Effects in Polymeric Solids; Wiley: New York, 1967.
17. Zhou, H., Wilkes, G. L. Macromolecules 1997, 30, 2412.
18. Celgard Corp. LLC, product literature.
19. Aharoni, S. M., Sibilia, J. P. Polym Eng Sci 1979, 19, 450.
20. Porter, R. S., Wang, L. J Macromol Sci Rev Macromol Chem Phys C 1995, 35, 63.
21. Uehara, H., Jounai, K., Endo, R., Okuyama, H., Kanamoto, T., Porter, R. S. Polym J 1997, 29, 198.
22. Celgard Corp. LLC., private communication.
23. Hermans, P. H., Hermans, J. J., Vermaas, D., Weidinger, A. J Polym Sci 1947, 3, 1.
24. He, T., Porter, R. S. Polymer 1987, 28, 946.
25. Gabbay, S. M., Stivala, S. S. Polymer 1976, 17, 121.
26. Zhou, H., Wilkes, G. L. J Mater Sci 1998, 33, 287.
27. Choy, C. L., Luk, W. K., Chen, F. C. Polymer 1981, 22, 543.
28. Lopez, L. C., Wilkes, G. L., Stricklen, P. M., White, S. A. JMS-Rev Macromol Chem Phys C 1992, 32(3,4), 301.